Acta Crystallographica Section A
Foundations of Crystallography
ISSN 0108-7673

Received 2 December 2008
Accepted 11 February 2009

Temperature-dependent Debye–Waller factors for semiconductors with the wurtzite-type structure

M. Schowalter,[a]* A. Rosenauer,[a] J. T. Titantah[b] and D. Lamoen[b]

[a]Institut für Festkörperphysik, Universität Bremen, D 28359 Bremen, Germany, and [b]EMAT, Universiteit Antwerpen, B-2400 Antwerpen, Belgium. Correspondence e-mail: schowalter@ifp.uni-bremen.de

We computed Debye–Waller factors in the temperature range from 0.1 to 1000 K for AlN, GaN, InN, ZnO and CdO with the wurtzite-type structure. The Debye–Waller factors were derived from phonon densities of states obtained from Hellmann–Feynman forces computed within the density-functional-theory formalism. The temperature dependences of the Debye–Waller factors were fitted and fit parameters are given.

1. Introduction

Wurtzite-type III–V semiconductors such as GaN have recently attracted a lot of interest due to the ability of GaN-based optoelectronic devices to cover the whole visible spectral range (Nakamura *et al.*, 1994). The wurtzite-type material ZnO is also of interest due to the large binding energy of the excitons in this material (Özgür *et al.*, 2005). In order to create high-performance devices based on these materials, a detailed analysis of the elemental distribution of the layers on an atomic scale is required. One of the methods of choice for investigating small semiconductor heterostructures on an atomic scale is transmission electron microscopy (TEM). Several methods have been developed for the quantification of composition in semiconductor heterostructures (Rosenauer, 2003). One widely used method is strain-state analysis, where the distances between atomic columns are measured from lattice-fringe images (Bierwolf *et al.*, 1993; Rosenauer *et al.*, 1996). However, this method suffers from artifacts due to the imaging process in TEM (Rosenauer *et al.*, 2006). Another method is the composition evaluation of lattice-fringe analysis (CELFA), which is not applicable to wurtzite-type materials due to the lack of a chemically sensitive reflection. Recently, Grillo *et al.* (2008) showed that the composition in InGaAs layers can be quantified from *Z*-contrast images using scanning transmission electron microscopy (STEM) in combination with a high-angle annular dark-field detector. Recently, Rosenauer *et al.* (2008) have shown that this method combined with measurement of normalized intensities allows measurement of the Al concentration in AlGaN/GaN heterostructures. However, the quantification is based on a comparison of experimental intensities with simulated intensities. For the simulation of *Z*-contrast images, thermal diffuse scattering plays an essential role and therefore the mean-square displacements of the atoms in the TEM specimen have to be known accurately.

Despite the wide interest in wurtzite-type semiconductors due to their technological importance, we were only able to find experimental phonon dispersion relations for AlN (Schwoerer-Böhning *et al.*, 1999) and ZnO (Serrano *et al.*, 2007). Phonon frequencies at the Γ point were measured for InN by Davydov *et al.* (1999) and for GaN (Lemos *et al.*, 1972; Filippidis *et al.*, 1996; Giehler *et al.*, 1995; Tabata *et al.*, 1996; Cros *et al.*, 1997). In contrast, several authors have computed phonon dispersion relations for GaN, AlN and InN (Bungaro *et al.*, 2000; Parlinski & Kawazoe, 1999; Siegel *et al.*, 2006; Manjon *et al.*, 2008; Schwoerer-Böhning *et al.*, 1999; Serrano *et al.*, 2007) using different first-principles approaches. However, we could not find any computation of Debye–Waller factors for these materials and we only found measurements for GaN by Xiong & Moss (1997) and for GaN and AlN by Schulz & Thiemann (1977).

In this paper we compute Debye–Waller factors in the temperature range from 0.1 to 1000 K for AlN, GaN, InN, ZnO and CdO with the wurtzite crystal structure. The temperature dependence is fitted using an approach published recently (Schowalter *et al.*, 2009). In §2 we briefly describe the computation of the Debye–Waller factors. For a detailed description of theory and computations of Debye–Waller factors the reader is referred Schowalter *et al.* (2009). Fit parameters for the temperature dependence of the Debye–Waller factors and a list of Debye–Waller factors at selected temperatures is given in §3 together with a short discussion of the results.

2. Description of the computations

In order to compute Debye–Waller factors one usually exploits the harmonic approximation, in which the Debye–Waller factor $B_{\alpha\beta}(\nu)$ can be derived from a generalized phonon density of states $g_{\alpha\beta}(\nu;\omega)$ by

$$B_{\alpha\beta}(\nu) = \frac{\hbar n}{16\pi^2 M_\nu} \int_0^\infty \mathrm{d}\omega \frac{\coth(\hbar\omega/2k_\mathrm{B}T)}{\omega} g_{\alpha\beta}(\nu;\omega), \quad (1)$$

Table 1
Comparison of calculated and experimental lattice parameters (Å).

Using the LDA (the GGA) the lattice parameters are underestimated (overestimated). Note that the DFT lattice parameters correspond to a temperature of 0 K, whereas the experimental lattice parameters were measured at 300 K. However, the thermal expansion of the lattice is negligible compared with the difference between the DFT and experimental lattice parameters.

Material	Lattice parameter	*WIEN2k*		Experiment	*ABINIT*	
		LDA	GGA		LDA	GGA
AlN	*a*	3.084	3.126	3.104	3.053	3.121
	c	4.991	5.059	4.966	4.942	5.053
GaN	*a*	3.153	3.216	3.209	3.035	3.252
	c	5.146	5.247	5.185	4.948	5.309
InN	*a*	3.497	3.569	3.548	3.518	3.600
	c	5.690	5.810	5.760	5.729	5.860
ZnO	*a*	3.182	3.271	3.250	3.214	3.308
	c	5.176	5.313	5.267	5.231	5.377
CdO	*a*	3.542	3.645	—	3.589	3.695
	c	5.732	5.909	—	5.823	5.993

where n is the number of phonon branches, M_ν is the mass of atom ν, ω is the phonon frequency, T is the temperature and k_B and $\hbar$ are Boltzmann's constant and Planck's constant divided by 2π, respectively. The indices α and β run over the three directions given by the lattice basis vectors. The Debye–Waller factor is in general a matrix. The phonon frequencies for the phonon density of states were derived by Fourier-transforming force-constant matrices, yielding the dynamical matrix. Phonon frequencies and phonon eigenvectors for the generalized phonon density of states can be calculated by diagonalizing the dynamical matrix.

The force-constant matrices were computed within the density-functional-theory (DFT) formalism using the *WIEN2k* code (Blaha *et al.*, 2001) and the *PHONON* program of Parlinski *et al.* (1997). In the first step the lattice parameters are computed, since lattice parameters are usually overestimated or underestimated within DFT depending on the approximation made for the exchange and correlation part of the potential. Applying an experimental lattice parameter would mean for DFT that the simulated crystal is under pressure and net forces are acting on the atoms. Therefore, we computed the energy as a function of the *a* and *c* lattice parameters for each material. In the vicinity of the minimum we fitted a paraboloid to the dependence of the energy on the lattice parameters. Using the optimized lattice parameters, 12 supercells were generated from the primitive supercell for each material. We used rhombohedral supercells with 48 atoms and with basis vectors of the rhombohedral cell $\mathbf{a}_r = 2\mathbf{a} + \mathbf{c}$, $\mathbf{b}_r = 2\mathbf{b} + \mathbf{c}$ and $\mathbf{c}_r = -2\mathbf{a} - 2\mathbf{b} + \mathbf{c}$ with **a**, **b** and **c** being the basis vectors of the hexagonal cell as used by Parlinski & Kawazoe (1999) to compute the phonon-dispersion relation of GaN. Then one of the atoms was displaced by 3 pm in each supercell and the Hellmann–Feynman forces on all the atoms were computed using the *WIEN2k* code. From the Hellmann–Feynman forces and the respective displacement, force-constant matrices were calculated with *PHONON* and phonon-dispersion relations and phonon densities of states were generated.

Table 2
Born effective charges (e) of the cations and dielectric functions at infinite frequency.

Material	LDA			GGA		
	Z_1^*	Z_3^*	ε_∞	Z_1^*	Z_3^*	ε_∞
AlN	2.53	2.66	4.41	2.53	2.66	4.55
GaN	2.59	2.71	4.90	2.69	2.71	6.6
InN	3.01	3.02	18.87	3.06	3.12	23.98
ZnO	2.19	2.20	5.93	2.23	2.25	5.99
CdO	3.05	2.38	43.01	2.75	2.41	25.23

In order to take into account the mixed ionic nature of the chemical bonding in these materials, which influences the optical phonon frequencies at the Γ point, we computed Born effective charges and the dielectric function at infinite frequency using density-functional perturbation theory using the *ABINIT* code (Gonze *et al.*, 2002). Then the non-analytical contribution was added to the analytical part of the dynamical matrix as described by Parlinski & Kawazoe (1999).

For the computations within *WIEN2k* we took about 100 *k*-points in the full Brillouin zone depending on the material; the plane wavevector cutoff K_{max} was set in such a way that $R_{MT}K_{max} = 7$, where R_{MT} is the radius of the muffin-tin spheres around the atom positions. (The *WIEN2k* code uses a spherical harmonics basis set within the muffin-tin spheres and plane waves in the interstitial region.) This ensured that the phonon frequencies converged to a precision of better than 1%.

For the computation of the Born effective charges within *ABINIT* we used a $7 \times 7 \times 5$ Monkhorst–Pack *k*-point mesh (Monkhorst & Pack, 1976) and a cutoff energy for the plane-wave expansion of about 40–60 hartree depending on the material. In contrast to the full-potential all-electron code *WIEN2k*, the *ABINIT* code uses pseudopotentials in the vicinity of the cores of the atoms. For our computations we used norm-conserving pseudopotentials generated according to the Troullier–Martins scheme (Troullier & Martins, 1991) with the *FHI* code provided on the web page of the *ABINIT* code at http://www.abinit.org.

3. Results and discussion

Table 1 compares the lattice parameters that were computed using the *WIEN2k* code and the *ABINIT* code with experimental lattice parameters, since the computation of the Hellmann–Feynman forces and the Born effective charges requires that the lattice parameters used are computed within the same code. The values exhibit the well known overbinding or underbinding when local density approximation (LDA) or generalized gradient approximation (GGA) is used for the exchange and correlation part of the potential. In Table 2 we show the computed Born effective charges and dielectric functions at infinite frequencies for the materials under discussion here. The computed phonon-dispersion relations along high-symmetry directions of AlN are compared with measured phonon frequencies (red dots) in Fig. 1. The experimental values were taken from Schwoerer-Böhning *et*

al. (1999). The black lines show the dispersion relation derived from Hellmann–Feynman forces computed within the GGA and the green dashed lines show the dispersion relation derived from Hellmann–Feynman forces computed within the LDA. In particular, the optical phonon frequencies computed within the LDA seem to fit better with the experimental frequencies than the frequencies computed within the GGA. The generalized phonon densities of states necessary for the calculation of the temperature dependence of the Debye–Waller factors according to equation (1) were computed using

$$g_{\alpha\beta}(\nu;\omega) = (1/\Delta\omega r)\sum_{\mathbf{k},\lambda} e_{\alpha}(\nu;\mathbf{k},\lambda)e^{*}_{\beta}(\nu;\mathbf{k},\lambda)\delta_{\Delta\omega}[\omega-\omega(\mathbf{k},\lambda)], \tag{2}$$

where α and β label the crystallographic directions, $\mathbf{e}(\nu;\mathbf{k},\lambda)$ is the λth eigenvector of non-equivalent atom ν resulting from the diagonalization of the dynamical matrix belonging to wavevector $\mathbf{k}$ and $\Delta\omega$ is the width of the frequency channel of the function $\delta_{\Delta\omega}(\omega)$ that is defined as

$$\delta_{\Delta\omega}(\omega) = \begin{cases} 1 & -\Delta\omega/2 < \omega \leq \Delta\omega/2 \\ 0 & \text{otherwise} \end{cases}. \tag{3}$$

For the final calculations we used 1 000 000 $\mathbf{k}$ vectors and a frequency-channel width of $\Delta\omega$ = 0.01 THz. Fig. 2 shows the total phonon density of states for AlN, which can be calculated by summing over all the components of the generalized phonon densities of states and the non-equivalent atoms ν.

The Debye–Waller factor is related to the static correlation function by

$$B_{\alpha\beta}(\nu) = 8\pi^2\langle u_{\alpha}(\nu)u_{\beta}(\nu)\rangle, \tag{4}$$

where $u_{\alpha}(\nu)$ is the displacement of atom ν in direction α. The temperature dependences of the static correlation functions were computed from the generalized phonon densities of states using equation (1). In Fig. 3 the isotropic static correlation functions $\langle u^2(\nu)\rangle = 2\langle u^2_{11}(\nu)\rangle + \langle u^2_{33}(\nu)\rangle$ are shown for Al and N. We only show the isotropic static correlation functions because the anisotropy is negligible for Al and N in AlN according to our computations. The lines in Fig. 3 are fit curves using the function (Schowalter *et al.*, 2009)

$$\langle u^2(\nu;T)\rangle = \frac{\hbar}{2M_{\nu}}\frac{\coth\{\hbar[A\exp(-T^2/\sigma^2)+B]/2k_{\mathrm{B}}T\}}{[A\exp(-T^2/\sigma^2)+B]}, \tag{5}$$

where k_{B} is Boltzmann's constant, and A, B and σ are fit parameters to the computed temperature dependence of the static correlation function. Equation (5) was used to obtain a least-squares fit. The resulting values for A, B and σ are given in Tables 3 and 4 for computations based on Hellmann–Feynman forces computed within the LDA (upper half of both tables) and the GGA (lower half of both tables).

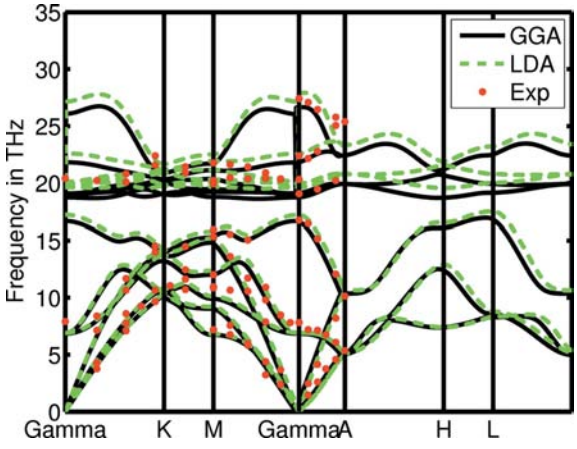

Figure 1
Comparison of computed phonon-dispersion relations for AlN derived from Hellmann–Feynman forces computed within the GGA (black lines) and the LDA (green dashed lines) with measured phonon frequencies (red dots) taken from Schwoerer-Böhning *et al.* (1999).

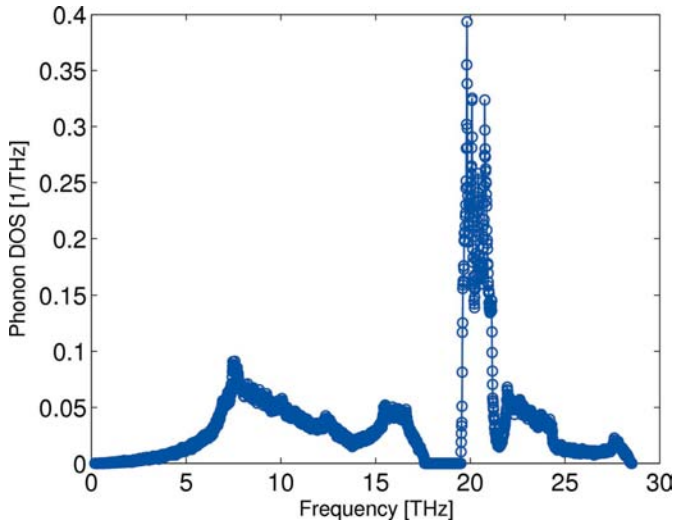

Figure 2
Total phonon density of states (DOS) for AlN derived from Hellmann–Feynman forces computed within the LDA.

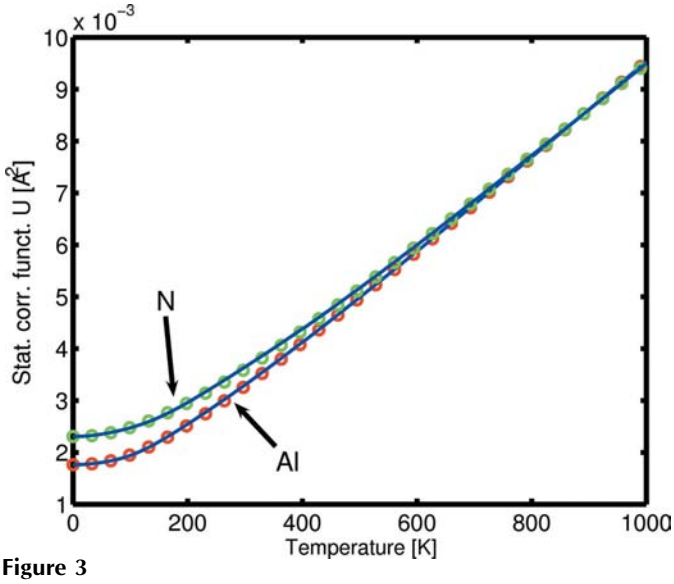

Figure 3
Temperature dependence of the isotropic static correlation functions for Al and N in AlN computed within the LDA.

Table 3
Fit parameters for the temperature dependence of the static correlation function.

The static correlation function is given by $\langle u_{11}^2(\nu; T)\rangle = \langle u_{22}^2(\nu; T)\rangle$, where ν can be either the metal or the nonmetal atom of the compound. Fits to values computed within the LDA are given in the first half of the table and fits to values computed within the GGA are given in the second half of the table.

Material	Element	σ (K)	A (Hz)	B (Hz)
AlN	Al	113.46935	6.719897e13	5.759433e13
	N	147.80605	9.776868e13	8.002983e13
GaN	Ga	66.66977	3.762785e13	3.297030e13
	N	130.70418	9.831563e13	7.523992e13
InN	In	38.70282	2.291791e13	1.942390e13
	N	94.15073	8.297150e13	5.620831e13
ZnO	Zn	33.63763	2.574266e13	1.911275e13
	O	65.99717	6.777918e13	4.064199e13
CdO	Cd	16.90255	1.456155e13	9.814533e12
	O	40.93614	5.584544e13	2.676237e13
AlN	Al	110.91858	6.546674e13	5.6409688e13
	N	144.43440	9.507914e13	7.8441558e13
GaN	Ga	63.86344	3.600160e13	3.1620503e13
	N	125.07103	9.352027e13	7.2158360e13
InN	In	37.56410	2.215029e13	1.8883193e13
	N	91.23950	7.901460e13	5.4534718e13
ZnO	Zn	29.25906	2.469921e13	1.7657970e13
	O	58.40570	6.399017e13	3.7589948e13
CdO	Cd	14.03687	1.506419e13	9.0389858e12
	O	34.85217	5.447520e13	2.4484793e13

Table 4
Fit parameters for the temperature dependence of the static correlation function $\langle u_{33}^2(\nu; T)\rangle$.

Fits to values computed within the LDA are given in the first half of the table and fits to values computed within the GGA are given in the second half of the table.

Material	Element	σ (K)	A (Hz)	B (Hz)
AlN	Al	114.42210	6.59189e13	5.67545e13
	N	150.86740	9.93236e13	8.08150e13
GaN	Ga	67.74198	3.74050e13	3.30493e13
	N	133.74860	9.99042e13	7.69262e13
InN	In	40.31723	2.27744e13	1.95978e13
	N	97.14156	8.41391e13	5.74111e13
ZnO	Zn	39.54738	2.60261e13	2.06822e13
	O	75.69874	6.90109e13	4.44722e13
CdO	Cd	12.29446	1.43220e13	8.09614e12
	O	30.42672	5.61220e13	2.20003e13
AlN	Al	112.91835	6.45692e13	5.60471e13
	N	148.75370	9.69517e13	7.98372e13
GaN	Ga	64.99992	3.57093e13	3.16483e13
	N	128.11385	9.50131e13	7.37487e13
InN	In	39.47486	2.20750e13	1.91626e13
	N	94.87927	8.02184e13	5.60907e13
ZnO	Zn	36.43394	2.48058e13	1.96440e13
	O	70.57320	6.50269e13	4.24149e13
CdO	Cd	12.91872	1.46399e13	8.60028e12
	O	32.63253	5.43278e13	2.33745e13

Explicit values for the static correlation function at selected temperatures are given in Table 5. Comparing the components $\langle u_{11}^2(\nu)\rangle$ and $\langle u_{33}^2(\nu)\rangle$ shows that there is only a small anisotropy in the Debye–Waller factors for AlN, GaN and InN, as mentioned before. This is in agreement with the measurement of Xiong & Moss (1997), who found only a small anisotropy in the Debye–Waller factors for Ga in GaN. A negligible anisotropy for AlN was observed by Schulz & Thiemann (1977), whereas the same authors reported a significant anisotropy for GaN. Unfortunately, neither publication states explicitly the temperature at which experiments were performed. However, assuming that the experiments were performed at 300 K, we compare their results with our computed static correlation functions in Table 6. Our values are in reasonable agreement with the measurements by Xiong & Moss (1997) for GaN and with measurements for AlN by Schulz & Thiemann (1977). However, a large difference is observed between our results

Table 5
Computed values of the static correlation function $\langle u_{11}^2(\nu; T)\rangle$ and $\langle u_{33}^2(\nu; T)\rangle$ (Å^2) at selected temperatures.

Values computed within the LDA are given in the first half of the table and values computed within the GGA are given in the second half of the table.

		ν = metal		ν = nonmetal	
Material	T (K)	$\langle u_{11}^2(\nu)\rangle$	$\langle u_{33}^2(\nu)\rangle$	$\langle u_{11}^2(\nu)\rangle$	$\langle u_{33}^2(\nu)\rangle$
AlN	0.001	0.001741	0.001766	0.002301	0.002258
	150.000	0.002169	0.002171	0.002678	0.002596
	300.000	0.003217	0.003215	0.003582	0.003443
	500.000	0.004881	0.004877	0.005118	0.004893
	1000.000	0.009329	0.009321	0.009428	0.008980
GaN	0.001	0.001203	0.001205	0.002285	0.002249
	150.000	0.001974	0.001928	0.002849	0.002739
	300.000	0.003433	0.003339	0.003937	0.003727
	500.000	0.005523	0.005366	0.005708	0.005359
	1000.000	0.010875	0.010560	0.010606	0.009909
InN	0.001	0.001207	0.001210	0.002734	0.002688
	150.000	0.003092	0.003019	0.004206	0.004053
	300.000	0.005851	0.005706	0.006485	0.006200
	500.000	0.009628	0.009386	0.009917	0.009445
	1000.000	0.019152	0.018668	0.019009	0.018067
ZnO	0.001	0.001874	0.001832	0.002902	0.002834
	150.000	0.005353	0.004132	0.005754	0.004517
	300.000	0.010135	0.007694	0.009701	0.007235
	500.000	0.016678	0.012609	0.015367	0.011258
	1000.000	0.033172	0.025034	0.030005	0.021788
CdO	0.001	0.001931	0.001986	0.003545	0.003546
	150.000	0.011592	0.014460	0.012062	0.014799
	300.000	0.022839	0.028576	0.022191	0.027690
	500.000	0.03794	0.047501	0.036161	0.045331
	1000.000	0.075772	0.094894	0.071586	0.089927
AlN	0.001	0.001788	0.001814	0.002366	0.002324
	150.000	0.002238	0.002241	0.002758	0.002676
	300.000	0.003339	0.003340	0.003703	0.003564
	500.000	0.005081	0.005082	0.005311	0.005083
	1000.000	0.009727	0.009730	0.009809	0.009356
GaN	0.001	0.001259	0.001263	0.002407	0.002368
	150.000	0.002126	0.002079	0.003031	0.002913
	300.000	0.003732	0.003637	0.004234	0.004009
	500.000	0.006020	0.005863	0.006186	0.005813
	1000.000	0.011869	0.011553	0.011556	0.010812
InN	0.001	0.001249	0.001253	0.002870	0.002824
	150.000	0.003274	0.003183	0.004432	0.004251
	300.000	0.006213	0.006031	0.006870	0.006526
	500.000	0.010232	0.009929	0.010545	0.009975
	1000.000	0.020360	0.019753	0.020261	0.019122
ZnO	0.001	0.001941	0.001907	0.003065	0.002992
	150.000	0.005851	0.004339	0.006230	0.004680
	300.000	0.011126	0.008101	0.010572	0.007482
	500.000	0.018328	0.013286	0.016804	0.011655
	1000.000	0.036471	0.026387	0.032874	0.022577
CdO	0.001	0.001877	0.001907	0.003641	0.003628
	150.000	0.013823	0.017129	0.014398	0.017666
	300.000	0.027298	0.033911	0.026792	0.033346
	500.000	0.045371	0.056391	0.043818	0.054744
	1000.000	0.090635	0.112675	0.086897	0.108748

Table 6
Comparison of computed static correlation functions $\langle u_{11}^2(\nu; T)\rangle$ and $\langle u_{33}^2(\nu; T)\rangle$ (Å^2) at room temperature with experimental data from the literature.

	ν = metal		ν = nonmetal	
	$\langle u_{11}^2(\nu)\rangle$	$\langle u_{33}^2(\nu)\rangle$	$\langle u_{11}^2(\nu)\rangle$	$\langle u_{33}^2(\nu)\rangle$
GaN				
LDA	0.0034	0.0033	0.0039	0.0037
GGA	0.0037	0.0036	0.0042	0.0040
Xiong & Moss (1997)	0.0036	0.0033	0.0048	0.0033
Schulz & Thiemann (1977)	0.0052	0.0027	0.0070	0.0024
AlN				
LDA	0.0032	0.0032	0.0036	0.0034
GGA	0.0033	0.0033	0.0037	0.0036
Schulz & Thiemann (1977)	0.0037	0.0040	0.0044	0.0046

and the measurements of Schulz & Thiemann for GaN. The group-III nitrides exhibit a large density of defects, such as threading dislocations and N-vacancies, which can modify the phonons substantially. Therefore, the experimental Debye–Waller factors can be modified due to the presence of defects in the crystal. An estimate of the effect of these defects on the Debye–Waller factors is beyond the scope of this paper.

As mentioned at the start of this section, the lattice parameters are under- or overestimated depending on the approximation (the LDA or the GGA) that is used for the computation within the density-functional-theory formalism. This means that the LDA leads to overbinding and the GGA to underbinding. The Debye–Waller factors should follow this trend (Vila *et al.*, 2007). Therefore, the Debye–Waller factor can be approximated by the average of the Debye–Waller factors computed within the LDA and the GGA. All the computations converged to such a precision that the maximum error on the Debye–Waller factor is given by the difference of the Debye–Waller factors computed within the LDA and the GGA.

4. Summary

In summary, we have computed phonon-dispersion relations for wurtzite-type III–V and II–VI semiconductors and have compared the phonon frequencies with values from the literature. We also derived phonon density of states for these materials and computed the Debye–Waller factors as a function of temperature. The temperature dependence has been fitted by a model function and the resulting parameters are given. The Debye–Waller factors calculated for GaN and AlN are in reasonable agreement with the literature.

This work was supported by the Deutsche Forschungsgemeinschaft under contract No. RO2057/4-1 and by the FWO-Vlaanderen under project G.0425.05. We have also benefited from computer time on the CalcUA supercomputer of the University of Antwerp. The authors also acknowledge financial support from the European Union under the Framework 6 program under a contract for an Integrated Infrastructure Initiative (reference 026019 ESTEEM). MS thanks A. Pretorius for encouragement to write this paper.

References

Bierwolf, R., Hohenstein, J., Phillipp, F., Brandt, O., Crook, G. E. & Ploog, K. (1993). *Ultramicroscopy*, **49**, 273–285.
Blaha, P., Schwarz, K., Madsen, G. K. H., Kvasnicka, D. & Luitz, J. (2001). *Wien2k, An augmented plane wave and local orbitals program for calculating crystal properties.* K. Schwarz, Technische Universität Wien, Austria. ISBN 3-9501031-1-2.
Bungaro, C., Rapcewicz, K. & Bernholc, J. (2000). *Phys. Rev. B*, **61**, 6720–6725.
Cros, A., Dimitrov, R., Angerer, H., Ambacher, O., Stutzmann, M., Christiansen, S., Albrecht, M. & Strunk, H. P. (1997). *J. Cryst. Growth*, **181**, 197–203.
Davydov, V. Yu., Klochikhin, A., Smirnov, M. B., Emtsev, V. V., Petrikov, V. D., Abroyan, I. A., Titov, A. I., Goncharuk, I. N., Smirnov, A. N., Mamutin, V. V., Ivanov, S. V. & Inushima, T. (1999). *Phys. Status Solidi B*, **216**, 779–783.
Filippidis, L., Siegle, H., Hoffmann, A., Thomsen, C., Karch, K. & Bechstedt, F. (1996). *Phys. Status Solidi B*, **198**, 621–627.
Giehler, M., Ramsteiner, M., Brandt, O., Yang, H. & Ploog, K. H. (1995). *Appl. Phys. Lett.* **67**, 733–735.
Gonze, X., Beuken, J.-M., Caracas, R., Detraux, F., Fuchs, M., Rignanese, G.-M., Sindic, L., Verstraete, M., Zerah, G., Jollet, F., Torrent, M., Roy, A., Mikami, M., Ghosez, Ph., Raty, J.-Y. & Allan, D. C. (2002). *Comput. Mater. Sci.* **25**, 478–492.
Grillo, V., Carlino, E. & Glas, F. (2008). *Phys. Rev. B*, **77**, 054103.
Lemos, V., Argello, C. A. & Leite, R. C. C. (1972). *Solid State Commun.* **11**, 1351–1353.
Manjon, F. J., Errandonea, D., Romero, A., Garro, N., Serrano, J. & Kuball, M. (2008). *Phys. Rev. B*, **77**, 205204.
Monkhorst, H. J. & Pack, J. D. (1976). *Phys. Rev. B*, **13**, 5188–5192.
Nakamura, S., Mukai, T. & Senoh, M. (1994). *Appl. Phys. Lett.* **64**, 1687–1689.
Özgür, Ü., Alivov, Y. I., Liu, C., Teke, A., Reshchikov, M. A., Doğan, S., Avrutin, V., Cho, S.-J. & Morkoç, H. (2005). *J. Appl. Phys.* **98**, 041301.
Parlinski, K. & Kawazoe, Y. (1999). *Phys. Rev. B*, **60**, 15511–15514.
Parlinski, K., Li, Z. Q. & Kawazoe, Y. (1997). *Phys. Rev. Lett.* **78**, 4063–4066.
Rosenauer, A. (2003). *Transmission Electron Microscopy of Semiconductor Nanostructures – An Analysis of Composition and Strain. Springer Tracts in Modern Physics*, No. 182. Heidelberg, Berlin: Springer.
Rosenauer, A., Gerthsen, D. & Potin, V. (2006). *Phys. Status Solidi A*, **203**, 176–184.
Rosenauer, A., Kaiser, S., Reisinger, T., Zweck, J. & Geb, W. (1996). *Optik*, **102**, 63–69.
Rosenauer, A., Schowalter, M., Pretorius, A., Dartsch, H., Figge, S., Hommel, D., Avramescu, A., Engl, K. & Lutgen, S. (2008). *Ultramicroscopy*. Submitted.
Schowalter, M., Rosenauer, A., Titantah, J. T. & Lamoen, D. (2009). *Acta Cryst.* A**65**, 5–17.
Schulz, H. & Thiemann, K. H. (1977). *Solid State Commun.* **23**, 815–819.
Schwoerer-Böhning, M., Macrander, A. T., Pabst, M. & Pavone, P. (1999). *Phys. Status Solidi B*, **215**, 177–180.
Serrano, J., Manjon, F. J., Romero, A., Ivanov, A., Lauck, R., Cardona, M. & Krisch, K. (2007). *Phys. Status Solidi B*, **244**, 1478–1482.
Siegel, A., Parlinski, K. & Wdowik, U. D. (2006). *Phys. Rev. B*, **74**, 104116.
Tabata, A., Enderlein, R., Leite, J. R., da Silva, S. W., Galzerani, J. C., Schikora, D., Kloidt, M. & Lischka, K. (1996). *J. Appl. Phys.* **79**, 4137–4140.
Troullier, N. & Martins, J. L. (1991). *Phys. Rev. B*, **43**, 1993–2006.
Vila, F. D., Rehr, J. J., Rossner, H. H. & Krappe, H. J. (2007). *Phys. Rev. B*, **76**, 014301.
Xiong, X. & Moss, S. C. (1997). *J. Appl. Phys.* **82**, 2308–2311.